Mononuclear and Dinuclear Ruthenium Complexes Containing the LRu(acac) Fragment. Crystal Structures of $[LRu^{III}(acac)(OH)]PF_6 \cdot H_2O$, $[\{LRu^{III}(acac)\}_2(\mu\text{-}O_2H_3)](PF_6)_3$, and $[\{LRu^{III}(acac)\}_2(\mu\text{-}O)](PF_6)_2$. Characterization of the Mixed-Valence Species $[\{LRu(acac)\}_2(\mu\text{-}O)](PF_6)_3$ (L = 1,4,7-Trimethyl-1,4,7-triazacyclononane)

Ralf Schneider, Thomas Weyhermüller, and Karl Wieghardt*

Lehrstuhl für Anorganische Chemie I, Ruhr-Universität, D-44780 Bochum, Germany

Bernhard Nuber

Anorganisch-Chemisches Institut der Universität, Im Neuenheimer Feld 270, D-69120 Heidelberg, Germany

Received April 8, 1993•

From a reaction mixture of $[LRuCl_3] \cdot H_2O$ (L = 1,4,7-trimethyl-1,4,7-triazacyclononane), sodium pentane-2,4-dionate (acac), and $NaPF_6$ in H_2O at pH >8 orange crystals of $[LRu(acac)(OH)]PF_6 \cdot H_2O$ (**1**) were obtained; a similar reaction in methanol affords $[LRu(acac)(OCH_3)][BPh_4]$ (**2**) when $NaBPh_4$ was added. When the reaction in H_2O was carried out at pH 6, violet crystals of $[\{LRu(acac)\}_2(\mu\text{-}O_2H_3)](PF_6)_3$ (**3**) precipitated. Heating of **1** in vacuo at 130 °C affords blue $[\{LRu(acac)\}_2(\mu\text{-}O)](PF_6)_2$ (**4**), which was recrystallized from toluene solution as a bis(toluene) solvate. **4** is readily oxidized by air or $Na_2[S_2O_8]$ in CH_3CN to yield red crystals of the mixed-valent form $[\{LRu^{3.5}(acac)\}_2(\mu\text{-}O)](PF_6)_3$ (**5**). The valences in **5** are delocalized. Electronic and ESR spectra of complexes **1–5** have been recorded, and the magnetic properties have been investigated. The electrochemistry has also been studied. Single-crystal X-ray structure determinations of **1**, **3**, and **4** have been carried out. Complex **1** crystallizes in the orthorhombic space group *Pcmb* with a = 8.431(2) Å, b = 16.178(4) Å, c = 16.478(4) Å, and Z = 4. The structure was solved by using 1926 observed reflections and refined to R_w = 0.064. Complex **3** crystallizes in the triclinic space group $P\bar{1}$ with a = 10.540(2) Å, b = 10.740(2) Å, c = 11.585(2) Å, α = 73.21(3)°, β = 79.83(3)°, γ = 65.61(3)°, and Z = 1. The structure was solved by using 3772 observed reflections and refined to R_w = 0.050. Complex **4** crystallizes in the triclinic space group $P\bar{1}$ with a = 10.762(3) Å, b = 11.570(6) Å, c = 12.562(4) Å, α = 117.02(3)°, β = 103.83(3)°, γ = 95.46(3)°, and Z = 1. The structure was solved by using 2593 observed reflections and refined to R_w = 0.067.

Introduction

In recent years oxoruthenium chemistry has been actively studied. Octahedral monooxoruthenium(IV)[1] and -(V)[2] and dioxoruthenium(VI)[3] complexes have been synthesized and in a few instances characterized by X-ray crystallography. On the other hand, corner-sharing μ-oxo-bridged dinuclear species containing a $Ru^{III}_2(\mu\text{-}O)$,[4-8] $Ru^{III}Ru^{IV}(\mu\text{-}O)$,[9-11] $Ru^{IV}_2(\mu\text{-}O)$,[12,13] or a $Ru^{V}_2(\mu\text{-}O)$[14] moiety have also been isolated or characterized in solution. In addition, higher-valent edge-sharing bis(μ-oxo)diruthenium[15] as well as face-sharing tris(μ-oxo)diruthenium(IV)[16] complexes have recently been described. These mononuclear and dinuclear oxo compounds have attracted a great deal of interest due to their potential as catalysts for the oxidation of organic substrates[17] or even water.[14,18]

We have begun to investigate the coordination chemistry of octahedral transition metal complexes containing a capping cyclic triamine such as 1,4,7-trimethyl-1,4,7-triazacyclononane (L) and, in addition, a bidentate pentane-2,4-dionate (acac) ligand.[19] The

• Abstract published in *Advance ACS Abstracts*, October 1, 1993.

(1) (a) Yukawa, Y.; Aoyagui, K.; Kurihara, M.; Shirai, K.; Shimizu, K.; Mukaida, M.; Takeuchi, T.; Kakihana, H. *Chem. Lett.* **1985**, 283. (b) Che, C. M.; Wong, K. Y.; Mak, T. C. M. *J. Chem. Soc., Chem. Commun.* **1985**, 546. (c) Dobson, J. C.; Helms, J. H.; Doppelt, P.; Sullivan, B. P.; Hatfield, W. E.; Meyer, T. J. *Inorg. Chem.* **1989**, *28*, 2200. (d) Moyer, B. A.; Meyer, T. J. *Inorg. Chem.* **1981**, *20*, 436.
(2) (a) Che, C.-M.; Yam, V. W.-W.; Mak, T. C. W. *J. Am. Chem. Soc.* **1990**, *112*, 2284. (b) Che, C.-M.; Lai, T.-F.; Wong, K.-Y. *Inorg. Chem.* **1987**, *26*, 2289.
(3) (a) Che, C. M.; Leung, W. H. *J. Chem. Soc., Chem. Commun.* **1987**, 1376. (b) El-Hendawy, A. M.; Griffith, W. P.; Piggott, D.; Williams, D. J. *J. Chem. Soc., Dalton Trans.* **1988**, 1983. (c) Perriers, S.; Lau, T. C.; Kochi, J. K. *Inorg. Chem.* **1992**, *29*, 4190. (d) Adeyami, S. A.; Dovletoglou, A.; Guadalupe, A. R.; Meyer, T. J. *Inorg. Chem.* **1992**, *31*, 1375.
(4) Baumann, J. A.; Meyer, T. J. *Inorg. Chem.* **1980**, *19*, 345.
(5) Weaver, T. R.; Meyer, T. J.; Adeyemi, S.; Brown, G. M.; Eckberg, R. P.; Hatfield, W. E.; Johnson, E. C.; Murray, R. W.; Untereker, D. *J. Am. Chem. Soc.* **1975**, *97*, 3039.
(6) Doppelt, P.; Meyer, T. J. *Inorg. Chem.* **1987**, *26*, 2027.
(7) Gilbert, J. A.; Eggleston, D. S.; Murphy, W. R.; Geselowitz, D. A.; Gersten, S. W.; Hodgson, D. J.; Meyer, T. J. *J. Am. Chem. Soc.* **1985**, *107*, 3855.
(8) Phelps, D. W.; Kahn, E. M.; Hodgson, D. J. *Inorg. Chem.* **1975**, *10*, 2486.
(9) Ikeda, M.; Shimizu, K.; Sato, G. P. *Bull. Chem. Soc. Jpn.* **1982**, *55*, 797.
(10) Baar, R. B.; Anson, F. C. *Electroanal. Chem. Interfacial Electrochem.* **1985**, *187*, 265.
(11) Zhou, J.; Xi, W.; Hurst, J. K. *Inorg. Chem.* **1990**, *29*, 160.
(12) (a) Masuda, H.; Taga, T.; Osaki, K.; Sugimoto, H.; Mori, M.; Ogoshi, H. *Bull. Chem. Soc. Jpn.* **1982**, *55*, 3887. (b) Masuda, H.; Taga, T.; Osaki, K.; Sugimoto, H.; Mori, M.; Yoshida, Z.; Ogoshi, H. *J. Am. Chem. Soc.* **1981**, *103*, 2199.
(13) (a) Mathieson, A. McL.; Mellor, D. P.; Stephenson, N. C. *Acta Crystallogr.* **1952**, *5*, 185. (b) Deloume, J. P.; Faure, R.; Thomas-David, G. *Acta Crystallogr., Sect. B: Struct. Crystallogr. Cryst. Chem.* **1979**, *B35*, 558.
(14) Geselowitz, D.; Meyer, T. J. *Inorg. Chem.* **1990**, *29*, 3894.
(15) Power, J. M.; Evertz, K.; Henling, L.; Marsh, R. E.; Schaefer, W. P.; Labinger, J. A.; Bercaw, J. E. *Inorg. Chem.* **1990**, *29*, 5058.
(16) Neubold, P.; Della Vedova, B. S. P. C.; Wieghardt, K.; Nuber, B.; Weiss, J. *Inorg. Chem.* **1990**, *29*, 3355.
(17) For a recent mechanistic study see: Roecker, L.; Meyer, T. J. *J. Am. Chem. Soc.* **1987**, *109*, 746.
(18) (a) Hurst, J. K.; Zhou, J.; Lei, Y. *Inorg. Chem.* **1992**, *31*, 1010. (b) Rotzinger, F.; Munavalli, S.; Comte, P.; Hurst, J. K.; Grätzel, M.; Pern, J.-F.; Frank, A. J. *J. Am. Chem. Soc.* **1987**, *109*, 6619. (c) Nazeeruddin, M. K.; Rotzinger, F. P.; Comte, P.; Grätzel, M. *J. Chem. Soc., Chem. Commun.* **1988**, 872.

0020-1669/93/1332-4925$04.00/0

Table I. Crystallographic Data for Complexes **1**, **3**, and **4**

	1	3	4
chem	$C_{14}H_{31}F_6N_3O_4PRu$	$C_{28}H_{59}F_{18}N_6O_6P_3Ru_2$	$C_{35}H_{64}F_{12}N_6O_5P_2Ru_2$
fw	551.4	1212.9	1141.0
space group	*Pcmb* (nonstandard setting of No. 57)	$P\bar{1}$ (No. 2)	$P\bar{1}$ (No. 2)
a, Å	8.431(2)	10.540 (2)	10.762(3)
b, Å	16.178(4)	10.740(2)	11.570(6)
c, Å	16.478(4)	11.585(2)	12.562(4)
α, β, γ, deg		73.21(3), 79.83(3), 65.61(3)	117.02(3), 103.83(3), 95.46(3)
V, Å^3	2248(2)	1141(4)	1315(1)
Z	4	1	1
ρ(calcd), g·cm^{-3}	1.63	1.765	1.44
temp, °C	22	22	22
radiation (λ, Å)	Mo Kα (0.710 73)	Mo Kα (0.710 73)	Mo Kα (0.710 73)
abs coeff, mm^{-1}	0.82	0.87	0.71
min/max transm coeff	0.713–0.771	0.253–0.292	0.92–1.00
R^a	0.071	0.045	0.078
Rw^a	0.064	0.050	0.067

[a] Residuals: $R = \sum|F_o - F_c|/\sum|F_o|$; $R_w = \{\sum w(F_o - F_c)^2/[\sum w(F_o)^2]\}^{1/2}$.

sixth ligand can then be water, hydroxide, or oxide depending on the d^n electron configuration of the metal ion. An oxo-bridged diiron(III) species has been isolated,[19c] and in the case of chromium(III) a symmetrical μ-O_2H_3-bridging group has been identified in $[\{LCr^{III}(acac)\}_2(\mu\text{-}O_2H_3^-)]^{3+}$ [19b] by X-ray crystallography. Here we report our results on such species containing an LRu(acac) fragment.

Experimental Section

The ligand 1,4,7-trimethyl-1,4,7-triazacyclononane (L)[20] and the starting material $LRuCl_3\cdot H_2O$[16] have been prepared as described previously.

Preparation of Complexes. [LRu(acac)(OH)](PF$_6$)·H$_2$O (1). Solid $LRuCl_3\cdot H_2O$ (2.0 g; 5.0 mmol) was added in small amounts to a solution of sodium 2,4-pentanedionate (acac) (3.0 g; ~24 mmol) in water (60 mL) with stirring at ambient temperature. The mixture was stirred for 3.5 h until a clear red solution was obtained. Addition of a solution of $NaPF_6$ (2.0 g) in H_2O (5 mL) and cooling to 0 °C initiated the precipitation of orange microcrystals of **1**, which were collected by filtration, washed with diethyl ether, and air-dried. Yield: 2.4 g (87%). Anal. Calcd for $C_{14}H_{31}N_3O_4F_6PRu$: C, 30.50; H, 5.67; N, 7.62. Found: C, 29.9; H, 5.5; N, 7.4.

[LRu(acac)(OCH$_3$)][BPh$_4$] (2). To a solution of Na(acac) (0.25 g; 2.0 mmol) in methanol (20 mL) was added $LRuCl_3\cdot H_2O$ (0.10 g; 0.25 mmol). The mixture was stirred at room temperature for 6.5 h until a clear red-orange solution was obtained. Addition of a solution of Na[BPh_4] (0.17 g; 0.50 mmol) in methanol (5 mL) initiated the rapid precipitation of orange microcrystals of **2**, which were collected by filtration, washed with methanol, and air-dried. Yield: 0.10 g (56%). Anal. Calcd for $C_{39}H_{51}BN_3O_3Ru$: C, 64.9; H, 7.1; N, 5.9. Found: C, 64.4; H, 7.1; N, 5.8.

[{LRu(acac)}$_2$(μ-O$_2$H$_3$)](PF$_6$)$_3$ (3). To an aqueous solution (20 mL) of 2,4-pentanedionate (1 mL; 9.7 mmol) was added $LRuCl_3\cdot H_2O$ (0.1 g; 0.25 mmol) and ammonium hydrogen carbonate (0.03 g; 0.38 mmol). The mixture was heated to reflux for 2 h. To the clear violet solution was added a solution of $NaPF_6$ (1.0 g; 5.9 mmol) in H_2O (3 mL), the pH of which had been adjusted to 6 by addition of HPF_6. Cooling to 0 °C initiated within a few hours the precipitation of violet crystals, which were collected by filtration, washed with a small amount of ice-cold H_2O, and air-dried. Yield: 0.10 g (86%). Anal. Calcd for $C_{28}H_{59}N_6F_{18}O_6P_3Ru_2$: C, 27.7; H, 4.9; N, 7.0. Found: C, 27.5; H, 4.9; N, 6.8.

[{LRu(acac)}$_2$(μ-O)](PF$_6$)$_2$ (4). [LRu(acac)(OH)PF_6]·H_2O (0.1 g; 0.19 mmol) in a small flask was slowly heated within 1.5 h to 130 °C *in vacuo* (oil pump vacuum). The temperature and the vacuum were maintained for 8 h, after which time the deep blue residue was repeatedly (2–3 times) recrystallized from a CH_3CN/toluene mixture (1:1). Alternatively purification was achieved by column chromatography (Al_2O_3; Merck II-III, 90) with CH_3CN/toluene mixtures with increasing CH_3CN concentrations as eluants. Yield: 0.09 g (90%). Anal. Calcd for $C_{28}H_{56}N_6F_{12}O_5P_2Ru_2$: C, 32.1; H, 5.4; N, 8.1. Found: C, 32.0; H, 5.3; N, 7.9. Single crystals of **4** suitable for an X-ray determination were slowly grown from a toluene solution. The product contains two molecules of toluene of crystallization per formula unit.

[{LRu(acac)}$_2$(μ-O)](PF$_6$)$_3$ (5). To a solution of **4** (0.40 g; 0.38 mmol) in CH_3CN (20 mL) was added an aqueous solution (5 mL) of $Na_2[S_2O_8]$ (0.05 g; 0.21 mmol). The solution was stirred at room temperature for 15 min, after which time a solution of $NaPF_6$ (2.0 g; 11.8 mmol) in a water/acetonitrile mixture (1:2) was added dropwise. All solvent was removed by rotary evaporation at ambient temperature. The residue was extracted with CH_3CN (15 mL) and filtered. The resulting solution was added dropwise to a cooled solution (−10 °C) of intensively stirred dry diethyl ether. In water very soluble red microcrystals precipitated, which were immediately collected by filtration, washed with cold dry diethyl ether, and dried in vacuo over P_4O_{10}. Yield: 0.32 g (71%). Anal. Calcd for $C_{28}H_{56}N_6F_{18}O_5P_3Ru_2$: C, 28.2; H, 4.7; N, 7.0. Found: C, 27.9; H, 4.6; N, 7.2.

Physical Measurements. Magnetic susceptibilities of powdered samples were measured in the temperature range 81–293 K by using the Faraday method or, alternatively, in the range 50–293 K by using a SQUID magnetometer (Quantum Design). Magnetic susceptibility data were corrected for underlying diamagnetism by using tabulated Pascal's constants. X-band ESR spectra were recorded on solid samples or frozen acetonitrile solutions on a Bruker ER 200 ESR spectrometer. Infrared spectra were measured on a Perkin-Elmer 1720 X FT-IR spectrometer (KBr disks). The UV/vis/near-IR spectra were recorded on a Perkin-Elmer Lambda 9 spectrophotometer.

The apparatus used for electrochemical measurements has been described previously.[21] Cyclic voltammograms (cv's) were usually recorded in acetonitrile (0.10 M tetra-*n*-butylammonium hexafluorophosphate, [TBA]PF_6, supporting electrolyte) under an argon atmosphere. At the beginning of each experiment a cv of the solution containing only the supporting electrolyte was recorded. To this solution were added solid samples (10^{-3}–10^{-4} M) and a nearly equimolar amount of ferrocene as internal standard.[22] The working electrode was either a Au, Pt, or glassy-carbon disk electrode; the reference electrode was a Ag/AgCl (saturated LiCl in C_2H_5OH) and a Pt wire auxiliary electrode. The redox potentials were measured against the internal standard ferrocenium/ferrocene (Fc^+/Fc) for which a redox potential in CH_3CN of 0.40 V vs the normal hydrogen electrode (NHE) was assumed. Criteria for the reversibility of electrode processes were those of Nicholson and Shain.[23]

X-ray Structure Determinations. Intensities and lattice parameters of a red prism of **1**, a red irregularly shaped crystal of **3**, and a blue-green platelet of **4** were measured on a Syntex R3 (**1**, **4**) or a Siemens P4 (**4**) diffractometer at ambient temperature by using monochromated Mo Kα radiation. Crystal parameters and details of the data collection and

(19) (a) Vanadium: Knopp, P.; Wieghardt, K.; Nuber, B.; Weiss, J. *Z. Naturforsch.* **1991**, *46b*, 1077. Knopp, P.; Wieghardt, K.; Nuber, B.; Weiss, J.; Sheldrick, W. S. *Inorg. Chem.* **1990**, *29*, 363. (b) Chromium: Bossek, U.; Wieghardt, K.; Nuber, B.; Weiss, J. *Angew. Chem.* **1990**, *102*, 1093; *Angew. Chem., Int. Ed. Engl.* **1990**, *29*, 1055. (c) Manganese and Iron: Wieghardt, K.; Pohl, K.; Bossek, U.; Nuber, B.; Weiss, J. *Z. Naturforsch.* **1988**, *43b*, 1184.

(20) Wieghardt, K.; Chaudhuri, P.; Nuber, B.; Weiss, J. *Inorg. Chem.* **1982**, *21*, 3086.

(21) Backes-Dahmann, G.; Herrmann, W.; Wieghardt, K.; Weiss, J. *Inorg. Chem.* **1985**, *24*, 485.

(22) Gagné, R. R.; Koval, C. A.; Lisensky, G. C. *Inorg. Chem.* **1980**, *19*, 2855.

(23) Nicholson, R. S.; Shain, I. *Anal. Chem.* **1964**, *36*, 706.

Scheme I. Synthesis of Complexes

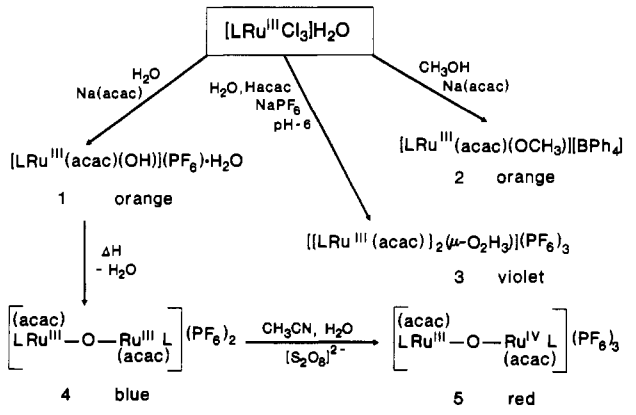

refinement are summarized in Table I (for full details see the supplementary material). Empirical absorption corrections (ψ-scans of seven reflections in the range $10 \leq 2\theta \leq 50°$) were carried out in each case. The structures of **1** and **4** were solved by conventional Patterson and difference Fourier methods whereas that of **3** was solved by direct methods. The Siemens program package (PC version) SHELXTL-PLUS was used. The function minimized during full-matrix least-squares refinement was $\sum w(|F_o| - |F_c|)^2$, where $w^{-1} = \sigma^2(F)$. Neutral-atom scattering factors and anomalous dispersion corrections for non-hydrogen atoms were taken from ref 24. The positions of hydrogen atoms of the methylene groups were placed at calculated positions with d(C–H) = 0.96 Å and isotropic thermal parameters, while the methyl groups were treated as rigid bodies, each with three rotational variables. For **1** the hydrogen atoms were not calculated. For **3** the final difference Fourier map revealed two chemically reasonable residual electron density peaks in the vicinity of oxygen atom O(1). These refined smoothly as hydrogen atoms with an occupancy factor of 1.0 for H(1) and of 0.5 for H(2). Thus H(2) is disordered over two positions related by a crystallographic center of symmetry indicating an asymmetric $(O_2H_3)^-$ bridge. The water molecule of crystallization in **1** refined with an occupancy factor of 0.5, indicating thereby a disorder of this molecule over two positions which are related by a crystallographic mirror plane. All non-hydrogen atoms were refined with anisotropic thermal parameters.

It is noted that the choice of space group of **1** is not unambiguous. Both the Hamilton R-test[25] and Roger's η-factor[26] were inconclusive. We have refined the structure in both the centric and acentric space group and decided that the centric space group is probably correct since the bond distances are chemically more reasonable than in the other refinement. The choice introduces crystallographic site symmetry m in the $[LRu(acac)(OH)]^+$ cation which is not compatible with the ($\lambda\lambda\lambda$) or ($\delta\delta\delta$) conformation of the five-membered Ru–N–C–C–N chelate rings of the coordinated cyclic amine. One CH_2–CH_2 group is therefore disordered. Attempts to model this by using a split atom model failed.

Results

Preparation, Magnetism, and Spectroscopic Characterization of Complexes. The synthetic routes employed are summarized in Scheme I. Spectroscopic data and magnetic properties of complexes **1**–**5** are given in Table II.

Reaction of solid $[LRuCl_3]\cdot H_2O$ with sodium pentane-2,4-dionate (acac) in water at ambient temperature produced a clear red solution from which upon addition of $NaPF_6$ orange microcrystals of $[LRu^{III}(acac)(OH)]PF_6\cdot H_2O$ (**1**) were obtained in 87% yield. When the same reaction was carried out in methanol and sodium tetraphenylborate was added, orange crystals of the methoxy derivative $[LRu^{III}(acac)(OCH_3)][BPh_4]$ (**2**) were obtained. Adjustment of the pH to 6 of the above aqueous reaction mixture caused a color change to violet. Addition of $NaPF_6$ and evaporation of the solvent initiated the precipitation of violet crystals of $[\{LRu^{III}(acac)\}_2(\mu\text{-}O_2H_3)](PF_6)_3$ (**3**).

When a solid sample of orange **1** was heated to 130 °C **in vacuo** for 8 h, a deep blue residue was obtained which after recrystallization from an acetonitrile/toluene mixture (1:1) produced deep blue crystals of $[\{LRu^{III}(acac)\}_2(\mu\text{-}O)](PF_6)_2$ (**4**). Species **4** was found to be readily oxidized by $Na_2[S_2O_8]$ and air (in the presence of protons) in an acetonitrile/water mixture to yield red microcrystalline $[\{LRu(acac)\}_2(\mu\text{-}O)](PF_6)_3$ (**5**), which is the mixed-valent one-electron oxidation product of **4**.

As the crystal structure determination of **1** clearly indicates (see below), **1** does not contain a coordinated terminal hydroxo ligand but a Ru^{III}–O_2H_3 moiety with a coordinated $O_2H_3^-$ ligand. This is also reflected in the infrared spectrum of **1** (KBr disk) in the 4000–3000-cm^{-1} region where the expected ν(OH) stretching frequency of M–OH units at 3500–3600 cm^{-1} is not detected but there is a broad band at ~3140 cm^{-1}. Two weak sharp bands at 3629 and 3563 cm^{-1} are probably due to overtones of the PF_6^- counteranion since they do not change positions upon deuteration of **1** whereas the broad band at 3140 cm^{-1} is shifted to 2100 cm^{-1}.

Figure 1 displays the UV/vis spectra of aqueous solutions of **1** at pH 1 and 10; data for an CH_3CN solution of **1** are summarized in Table II. The observed color change of the solution from red (pH 10) to blue (pH 1) is due to a protonation–deprotonation equilibrium eq 1. From a plot of the absorbance change at 480

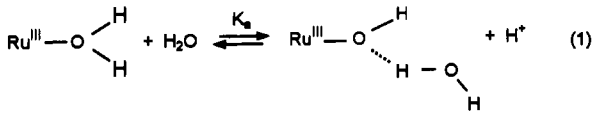

nm as a function of pH (inset Figure 1) we have calculated a dissociation constant. The pK_a value at 20 °C is ~5.8. Under our experimental conditions with [**1**] ~ 2×10^{-4} M the formation of **3** which is the μ_2-O_2H_3-bridged dinuclear species is assumed to be negligible. From the above spectra is followed that the d–d transition at 500 nm of **1**, which is observed at 477 nm in CH_3CN, is shifted to 550 nm upon protonation. This indicates that a coordinated $O_2H_3^-$ ligand exerts a slightly stronger ligand field than a coordinated water ligand. For the methoxo complex **2** the d–d transition in the visible is observed at ~490 nm (CH_3CN) indicating that the methoxo ligand has a ligand field of about the same strength as the $O_2H_3^-$ ligand.

The mononuclear complexes **1** and **2** contain a low-spin ruthenium(III) ion $(t_{2g})^5$. From temperature-dependent magnetic susceptibility measurements (81–298 K) slightly temperature dependent magnetic moments between 1.75 and 2.21 μ_B (Table II) are indicative of this electronic configuration ($S = {}^1/_2$). Figure 2 shows the X-band ESR spectrum of a polycrystalline sample of **1** at 4.2 K. An axial spectrum with $g_\parallel = 1.81$ and $g_\perp = 2.28$ ($g_{iso} = 2.12$) is observed.

As established by X-ray crystallography, **3** is a dinuclear complex where two $LRu^{III}(acac)$ fragments are bridged by a $O_2H_3^-$ moiety. The UV/vis spectrum of this species measured in dry CH_3CN displays a maximum at 569 nm, which does not correspond to either **1** or the protonated aquaruthenium(III) form thereof (or a superposition of both species). Addition of a drop of concentrated $HClO_4$ to this solution shifts the maximum to 550 nm, which indicated the formation of the mononuclear species $[LRu^{III}(acac)(OH_2)]^{2+}$. From temperature-dependent magnetic susceptibility measurements on a solid sample of **3** we calculate magnetic moments of 2.17 μ_B/Ru at 293 K and 1.85 μ_B/Ru at 81 K. Since these values are very similar to those observed for the genuine mononuclear species **1** and **2**, we conclude that the temperature dependence is due to spin–orbit coupling rather than intramolecular spin exchange coupling mediated by the $O_2H_3^-$ bridge in **3**. This is corroborated by the ESR spectrum of **3** in CH_3CN at 4.2 K shown in Figure 3 which displays a rhombic signal with $g_1 = 2.54$, $g_2 = 2.29$, and $g_3 = 1.64$ typical of an S

(24) *International Tables for X-ray Crystallography*; Kynoch: Birmingham, England, 1974; Vol. IV, pp 99, 149.
(25) Hamilton, W. C. *Acta Crystallogr.* **1965**, *18*, 502.
(26) Rogers, D. *Acta Crystallogr., Sect. A* **1981**, *A37*, 734.

Table II. Electronic and ESR Spectral Data and Magnetic Properties of Complexes **1–5**

complex	λ_{max}, nm (ϵ, L·mol^{-1}·cm^{-1})[a]	X-band ESR g-values	μ_{eff}, μ_B (temp, K)
1	275 (5.7 × 10^3), 316 sh, 355 (2.8 × 10^3), 477 sh (366)	2.28, 1.81[b]	1.75 (81), 1.95 (293)
2	267 (7.6 × 10^3), 274 (7.5 × 10^3), 341 (2.6 × 10^3) 389 (2.6 × 10^3), 490 sh (604)		1.80 (81), 2.21 (293)
3	278 (10.8 × 10^3), 312 (7.3 × 10^3), 365 sh, 485 sh, 569 (952)	2.54, 2.29, 1.64[c]	2.62 (81), 3.07 (293)
4	280 (10.6 × 10^3), 350 (4.6 × 10^3), 596 (12.4 × 10^3), 850 (310)	silent at 4.2 K	1.38 (81), 2.65 (295)
5	289 (8.8 × 10^3), 386 (8.9 × 10^3), 537 (5.7 × 10^3), 580 sh, 1309 (237)	2.47, 1.32, 0.88[b]	1.33 (80), 1.61 (295)

[a] Solvent: CH_3CN. [b] Polycrystalline sample at 4.2 K. [c] CH_3CN glass at 4.2 K.

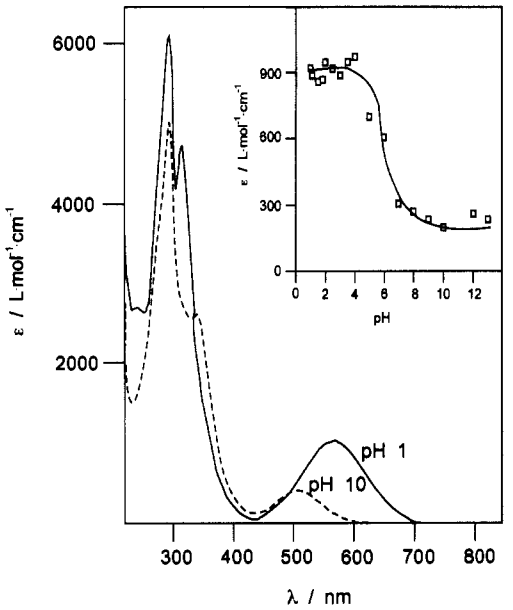

Figure 1. Electronic spectra of **1**: Aqueous solution at pH 1 ($HClO_4$) (—) and pH 10 (borate buffer) (- - -) at 20 °C ([**1**] = 2.9 × 10^{-4} M). The inset shows the pH dependence of the absorption at 480 nm. The solid line is drawn as a guide for the eyes only.

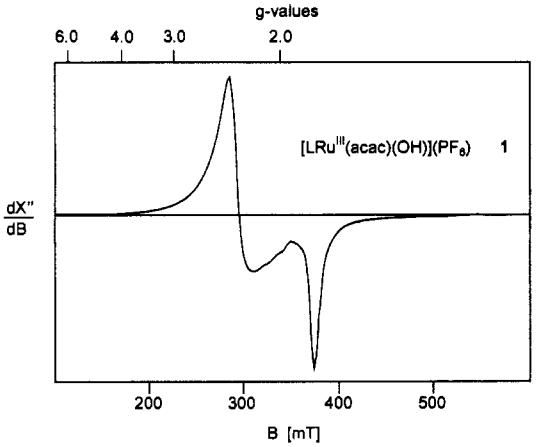

Figure 2. X-band ESR spectrum of a polycrystalline sample of **1** at 4.2 K (microwave 9.4387 GHz; 20 μW/40 dB; modulation 10.0 G).

= $^1/_2$ spin system. Intermolecular antiferromagnetic exchange coupling would give an $S = 0$ ground state which is clearly not observed.

Figure 4 shows the electronic spectra of the two μ-oxo-bridged complexes **4** and **5**; the inset shows the oxidation of **4** to **5** by oxygen, which is a clean transformation as is judged from the observation of an isosbestic point at 540 nm. Both spectra exhibit an intense charge-transfer absorption maximum in the visible at 596 and 537 nm indicative of the presence of the Ru^{III}–O–Ru^{III} or $Ru^{3.5}$–O–$Ru^{3.5}$ chromophore, respectively. Interestingly, the mixed-valent species **5** exhibits an absorption maximum at 1309 nm (ϵ = 237 L mol^{-1} cm^{-1}). The half-width at half-height, $\Delta\nu_{1/2}$, of this maximum (ν_{max} = 7640 cm^{-1}) is ~1500 cm^{-1}, which is substantially smaller than the calculated value of 4200 cm^{-1} using

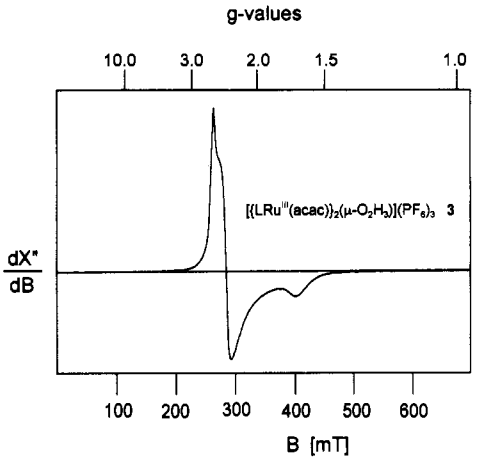

Figure 3. X-band ESR spectrum of an CH_3CN glass of **3** at 4.2 K (microwave 9.4322 GHz; 20 μW/40 dB; modulation 10.0 G).

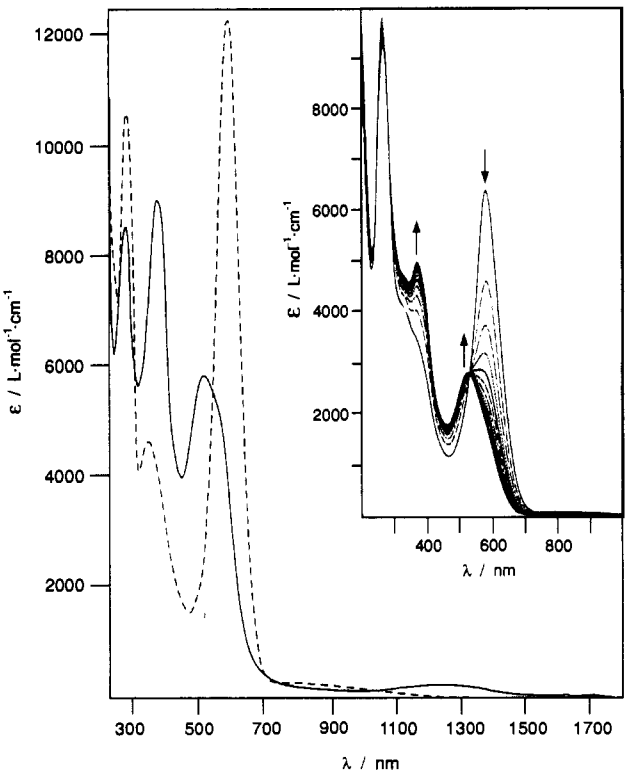

Figure 4. Electronic spectra of **4** (- - -) and **5** (—) in acetonitrile at 20 °C. The inset shows the oxidation o **4** to **5** by oxygen (scans were recorded at 60 min intervals).

the Hush relation (eq 2)[27a] for class II compounds according to

$$\Delta\nu_{1/2} = \sqrt{2300\nu_{max}} \qquad (2)$$

the Robin and Day[27b] classification. This points to a valence-

(27) (a) Hush, N. S. *Prog. Inorg. Chem.* **1967**, *8*, 391. (b) Robin, M. B.; Day, P. *Adv. Inorg. Chem. Radiochem.* **1967**, *10*, 247. (c) Crentz, C. *Prog. Inorg. Chem.* **1983**, *30*, 1.

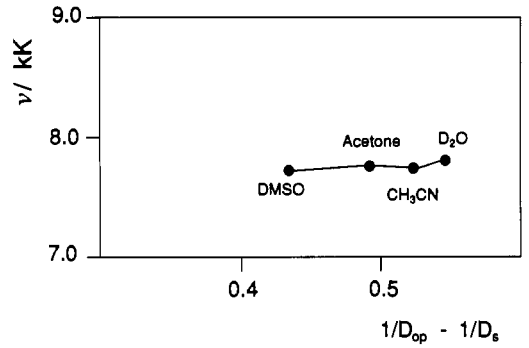

Figure 5. Plot of the energy of the intervalence band ν_{max} of **5** vs the difference of the reciprocal optical and stationary dielectric constants of the solvent.

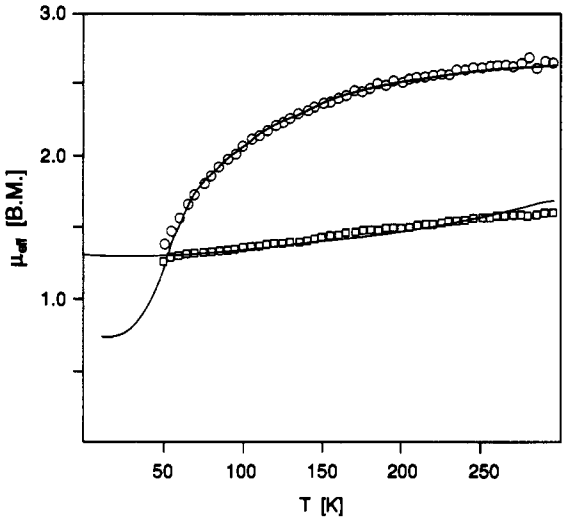

Figure 6. Temperature dependence of the magnetic moments of **4** (○) and **5** (□). Solid lines represent the best fits (see text).

delocalized $Ru^{3.5}$–O–$Ru^{3.5}$ system in **5** (class III). This is further corroborated by the observation that the energy of the intervalence band ν_{max} is independent of the polarity of the solvent as is shown in Figure 5.[27c]

Figure 6 shows the temperature dependence of the magnetic moments of **4** and **5** in the temperature range 50–298 K. For **4** a decrease of μ is observed from 2.65 μ_B at 298 K to 1.38 μ_B at 50 K. By using the isotropic Heisenberg model for spin exchange coupled dinuclear complexes with the spin Hamiltonian $H = -2JS_1S_2$, where $S_1 = S_2 = {}^1/_2$ for each ruthenium(III) ion, and by treating the coupling constant J, the g-value, and a small percentage of a mononuclear ruthenium(III) impurity P as variables, we fitted the susceptibility data successfully with $J = -53(2)$ cm^{-1}, $g = 2.22$, and $P = 4.8\%$. Thus the unpaired electrons at the ruthenium(III) centers are intramolecularly antiferromagnetically coupled. It is noted that the g-value of 2.22 obtained from the above fit compares well with the experimentally determined values for **1** and **3** (see above). This is taken as an indication that the simple Heisenberg model adequately describes the magnetic properties in the investigated temperature range.

The temperature dependence of the magnetic moment of **5** is relatively small. At 295 K μ is 1.61 μ_B and at 50 K a value of 1.28 μ_B is observed. These values are smaller than the spin-only value for one electron of 1.73 μ_B but indicate the presence of one unpaired electron per dinuclear unit. The solid line in Figure 6 represents an attempt to fit the temperature dependence of the magnetic moment of **5** by using the same isotropic Heisenberg model for exchange coupling between a Ru^{IV} ion ($S_1 = 1$) and a low-spin Ru^{III} ion ($S_2 = {}^1/_2$). A reasonable fit was obtained with $J = -157$ cm^{-1}, a g-value of 1.53, and $P = 0$. Thus the magnetic behavior of **5** may be modeled by a strong intramolecular antiferromagnetic exchange coupling as well as by a molecular

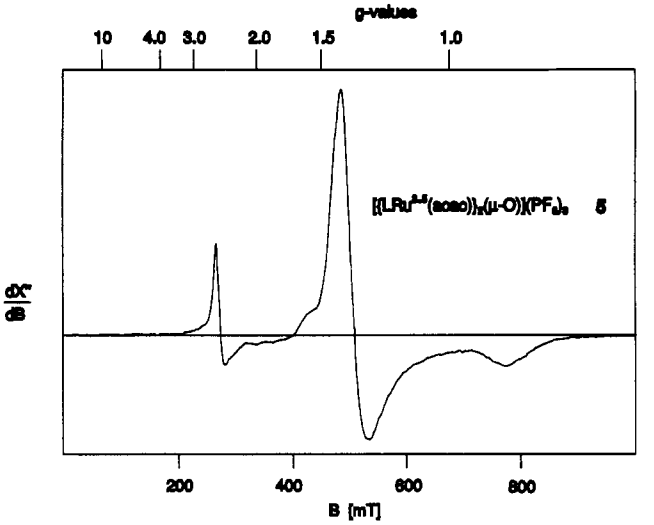

Figure 7. X-band ESR spectrum of a polycrystalline sample of **5** at 10 K (microwave 9.4397 GHz; 20 μW/40 dB; modulation 10 G).

Table III. Atomic Coordinates (×10^4) and Equivalent Isotropic Displacement Parameters (× 10^3) for **1**

atom	x	y	z	U(eq)
Ru(1)	2241(1)	2500	552(1)	44(1)
O(1)	3395(11)	2500	-489(6)	96(4)
O(2)	756(7)	1603(3)	148(3)	58(2)
C(1)	-1392(11)	954(6)	-524(6)	81(4)
C(2)	-542(11)	1741(6)	-275(5)	60(3)
C(3)	-1160(14)	2500	-494(8)	59(4)
N(1)	1254(10)	2500	1737(6)	51(3)
N(2)	3813(7)	1632(4)	1060(5)	59(3)
C(4)	1854(13)	1740(7)	2153(6)	103(5)
C(5)	3109(15)	1329(8)	1812(7)	128(6)
C(6)	5311(10)	2075(5)	1242(8)	115(5)
C(7)	-564(13)	2500	1732(8)	75(6)
C(8)	4129(12)	911(6)	503(7)	91(4)
P(1)	7828(6)	0	2500	142(3)
F(11)	7858(12)	357(7)	1609(7)	227(6)
F(12)	6028(13)	0	2500	302(12)
F(13)	9637(14)	0	2500	183(7)
F(14)	7872(14)	-925(6)	2206(9)	249(8)
O(3)	5048(24)	1688(11)	3549(11)	163(7)

orbital description (see Discussion) with an unpaired electron in a π_1* MO.[5] The origin of the unusually small g_{iso}-value is unclear. Interestingly, the unusual rather low g-value is experimentally verified by the X-band ESR spectrum of a polycrystalline sample of **5** at 10 K, which is displayed in Figure 7. A rhombic signal with $g_1 = 2.47$, $g_2 = 1.32$, and $g_3 = 0.88$ is detected giving a g_{iso} value of 1.56 in good agreement with the value derived from bulk magnetic susceptibility measurements. Thus both the magnetic moment and the ESR spectrum indicate an $S = {}^1/_2$ ground state of **5**.

Crystal Structure Determinations. The crystal structures of **1**, **3**, and **4** have been determined by X-ray crystallography. Tables III–V give the atom coordinates of **1**, **3**, and **4**, respectively. Table VI summarizes selected bond distances and angles of the respective cations. Figures 8–10 show the structures of the cations in crystals of **1**, **3**, and **4**, respectively.

In all three structures the ruthenium(III) ions are in a pseudooctahedral environment composed of a facially coordinated cyclic triamine, a bidentate pentane-2,3-dionate, and an oxygen donor atom of a hydroxo (or $O_2H_3^-$) in **1**, a bridging $O_2H_3^-$ ligand in **3**, and a bridging oxo ligand in **4**. The metrical details of the coordinated acac ligands are within experimental error identical in all three structures and agree well with those reported for $Ru^{III}(acac)_3$[28] and *trans*-$[Ru(acac)_2Cl_2]^-$.[28b] The same is true for the Ru^{III}–N bonds in **1** and **3**, which agree also nicely with

Table IV. Atomic Coordinates (×10⁴) and Equivalent Isotropic Displacement Coefficients (Å² × 10³) for **3**

atom	x	y	z	U(eq)[a]
Ru(1)	8238(1)	-3008(1)	-1853(1)	34(1)
O(1)	9581(3)	-3722(3)	-518(3)	44(1)
O(2)	6665(3)	-2366(3)	-640(3)	46(1)
O(3)	8164(3)	-4920(3)	-1421(3)	47(1)
N(1)	7005(4)	-2347(4)	-3312(3)	56(1)
N(2)	8265(4)	-981(3)	-2467(3)	45(1)
N(3)	9899(4)	-3494(4)	-3169(3)	51(1)
C(1)	5688(5)	-2625(6)	-2944(5)	74(1)
C(2)	8285(5)	-367(4)	-1462(4)	53(1)
C(3)	10964(5)	-4947(5)	-2825(5)	60(1)
C(4)	6661(6)	-829(5)	-3885(5)	79(1)
C(5)	6891(6)	-121(5)	-3053(5)	71(1)
C(6)	9500(6)	-1021(5)	-3335(5)	68(1)
C(7)	10547(5)	-2442(5)	-3224(5)	68(1)
C(8)	9355(6)	-3249(6)	-4353(4)	78(1)
C(9)	7944(6)	-3264(6)	-4167(4)	75(1)
C(10)	5298(5)	-2496(6)	1191(5)	74(1)
C(11)	6269(4)	-3187(5)	240(4)	51(1)
C(12)	6647(5)	-4610(5)	363(5)	60(1)
C(13)	7507(5)	-5384(5)	-465(5)	54(1)
C(14)	7705(6)	-6900(5)	-279(6)	82(1)
P(1)	5000	5000	5000	88(1)
F(1)	5672(6)	4551(6)	3811(4)	163(1)
F(2)	4726(7)	3628(5)	5515(5)	176(1)
F(3)	6384(6)	4369(7)	5574(6)	218(1)
P(2)	8006(2)	-781(1)	2146(1)	54(1)
F(4)	6736(3)	255(3)	1351(3)	83(1)
F(5)	8291(4)	-1927(3)	1406(3)	86(1)
F(6)	9285(4)	-1837(4)	2939(3)	96(1)
F(7)	9009(4)	-191(4)	1201(3)	92(1)
F(8)	7726(4)	349(4)	2881(4)	111(1)
F(9)	6999(4)	-1381(5)	3084(3)	115(1)

[a] Equivalent isotropic *U* defined as one-third of the trace of the orthogonalized U_{ij} tensor.

bond lengths in other Ru(III) complexes containing the LRu^{III} fragment.[16,29] In the following we shall not discuss these features further.

Crystals of **1** consist of the mononuclear cation $[LRu^{III}(acac)(O_2H_3)]^+$ and PF_6^- anions. The most salient feature of the structure is the presence of a terminal $H_3O_2^-$ ligand consisting of a Ru–OH moiety which is strongly bound to a water molecule via a short O–H···O contact (O···O = 2.442(8) Å).

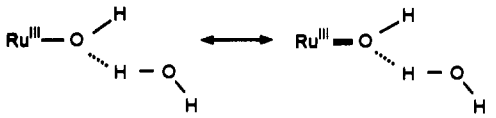

The positions of the hydrogen atoms were not located in the structure determination due to the disorder of the hydrogen-bonded water molecule. The $Ru–O_{hydroxo}$ bond distance at 1.971(9) Å is significantly shorter than $Ru–OH_2$ bonds in $[Ru^{III}(N_4O)(H_2O)](ClO_4)_2$ at 2.115(3) Å (N_4O represents bis-(2-(2-pyridyl)ethyl)(2-hydroxy-2-(2-pyridyl)ethyl)amine)[28a] or in $[\{(H_2O)(bpy)_2Ru^{III}\}_2O]^{4+}$ at 2.136(4) Å[7] or in $[Ru(H_2O)_6]^{3+}$ at 2.016–2.037 Å.[30] It resembles a $Ru–O_{alkoxo}$ distance at 1.961(4) Å as in $[Ru^{III}(N_4O)(H_2O)](ClO_4)_2$[28a] and indicates some ligand-to-metal $p_\pi \rightarrow d_\pi$ multiple bond character as shown in the two resonance structures above.

Crystals of **3** consist of the dinuclear μ-$H_3O_2^-$-bridged cation $[\{LRu(acac)\}_2(\mu\text{-}H_3O_2)]^{3+}$ and PF_6^- anions. The cation possesses crystallographically imposed C_i symmetry. The hydrogen atoms of the $H_3O_2^-$ bridge have been located in a difference Fourier map and were successfully refined. Interestingly, the $H_3O_2^-$ bridge does not possess C_i symmetry; the hydrogen atom H(2) does not lie on the center of symmetry but is distributed over two sites with an occupancy of 0.5. This indicates that the $H_3O_2^-$ bridge is asymmetric shown as follows:

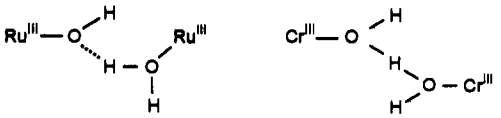

This is in contrast to the previously described chromium(III) analogue $[\{LCr(acac)\}_2(\mu\text{-}H_3O_2)]^{3+}$, where the $H_3O_2^-$ bridge was found to be centrosymmetric (O···O = 2.496(6) Å).[19b] Comparison of the terminal $H_3O_2^-$ ligand in **1** with the bridging in **3** shows that hydrogen bonding O–H···O contact at 2.494(7) Å in **3** is slightly weaker in **3** than in **1**. Concomitantly, the Ru–O

Table V. Atomic Coordinates (×10⁴) and Equivalent Isotropic Displacement Parameters (Å² × 10³) for $C_{28}H_{56}F_{12}N_6O_5P_2Ru_2$ (**4**)

atom	x	y	z	U(eq)[a]
Ru(1)	1508(1)	1177(1)	1421(1)	62(1)
O(1)	0	0	0	61(5)
O(2)	2776(7)	667(7)	400(6)	75(5)
O(3)	1310(7)	2755(6)	1113(6)	72(4)
C(11)	4047(12)	693(14)	-890(11)	112(10)
C(12)	3128(11)	1268(15)	-150(10)	85(8)
C(13)	2713(12)	2394(13)	-152(10)	78(7)
C(14)	1887(13)	3062(11)	464(11)	79(7)
C(15)	1564(12)	4261(12)	353(10)	103(8)
N(1)	1797(9)	-242(9)	2007(8)	70(5)
N(2)	423(9)	1777(9)	2675(8)	69(5)
N(3)	3129(10)	2432(10)	3115(8)	81(6)
C(1)	705(15)	-390(13)	2498(13)	118(10)
C(2)	111(13)	666(15)	2927(14)	116(11)
C(3)	1280(16)	2993(15)	3831(12)	134(10)
C(4)	2589(17)	3232(16)	4093(14)	152(12)
C(5)	3782(15)	1517(18)	3431(16)	156(14)
C(6)	3090(15)	272(16)	3011(12)	129(11)
C(7)	1766(11)	-1583(11)	978(10)	86(7)
C(8)	-820(11)	2108(11)	2216(10)	85(7)
C(9)	4136(11)	3318(12)	3043(10)	99(8)
P(1)	2147(4)	7330(4)	4427(3)	91(2)
F(11)	1068(9)	6310(10)	4353(12)	201(9)
F(12)	2830(9)	7891(12)	5851(8)	199(8)
F(13)	1515(10)	6919(11)	3030(7)	195(8)
F(14)	3263(9)	8400(8)	4532(9)	161(7)
F(15)	1233(8)	8372(8)	4749(7)	148(6)
F(16)	3061(8)	6322(7)	4091(8)	145(6)
C(16)	6852(25)	5709(19)	2276(15)	111(11)
C(17)	7870(19)	6806(31)	2892(19)	122(14)
C(18)	7593(26)	8043(28)	3390(16)	139(16)
C(19)	6342(35)	8173(23)	3284(18)	146(16)
C(20)	5357(20)	7075(31)	2683(20)	135(15)
C(21)	5606(21)	5873(21)	2166(14)	123(13)
C(22)	7192(20)	4392(17)	1738(17)	220(20)

[a] Equivalent isotropic *U* defined as one-third of the trace of the orthogonalized U_{ij} tensor.

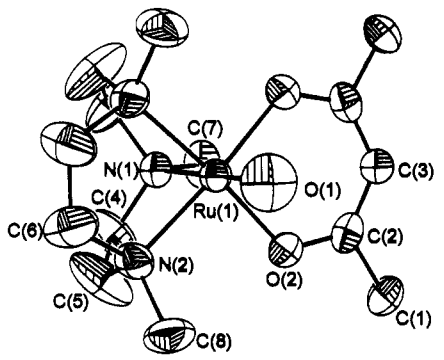

Figure 8. Structure of the cation in crystals of **1**. Atoms N(1), Ru(1), C(7), O(1), and C(3) lie on a crystallographic mirror plane.

(28) (a) Chao, G. K.-J.; Sime, R. L.; Sime, R. J. *Acta Crystallogr., Sect. B* **1973**, *B29*, 2845. (b) Hasegawa, T.; Lau, T. C.; Taube, H.; Schaefer, W. P. *Inorg. Chem.* **1991**, *30*, 2921.

(29) Neubold, P.; Wieghardt, K.; Nuber, B.; Weiss, J. *Inorg. Chem.* **1989**, *28*, 459.

(30) Dong, V.; Keller, H.-J.; Endres, H.; Moroni, W.; Nöthe, D. *Acta Crystallogr., Sect. B* **1977**, *B33*, 2428.

Table VI. Selected Bond Distances (Å) and Angles (deg) of Complexes **1**, **3**, and **4**

	Complex **1**		
Ru(1)–O(1)	1.971(9)	O(2)–C(2)	1.316(10)
Ru(1)–O(2)	2.029(5)	C(1)–C(2)	1.519(13)
Ru(1)–N(1)	2.124(9)	C(2)–C(3)	1.382(11)
Ru(1)–N(2)	2.106(7)	O(1)···O(3)	2.442(10)
O(1)–Ru(1)–O(2)	91.1(3)	O(2)–Ru(1)–N(2)	92.4(2)
O(1)–Ru(1)–N(1)	173.5(4)	N(1)–Ru(1)–N(2)	83.1(3)
O(2)–Ru(1)–N(1)	93.5(2)	O(1)–Ru(1)–O(2a)	91.1(3)
O(1)–Ru(1)–N(2)	92.0(3)	O(2)–Ru(1)–O(2a)	91.3(3)
N(2)–Ru(1)–O(2a)	175.1(3)	N(2)–Ru(1)–N(2a)	83.7(4)
	Complex **3**		
Ru(1)–O(1)	2.043(4)	Ru(1)–N(1)	2.091(5)
Ru(1)–O(2)	1.998(3)	Ru(1)–N(2)	2.097(4)
Ru(1)–O(3)	1.999(3)	Ru(1)–N(3)	2.103(4)
O(2)–C(11)	1.271(6)	O(3)–C(13)	1.282(7)
O(1)–H(1)	0.70(6)	O(1)–H(2)	0.98(10)
O(1)···O(1a)	2.494(7)		
O(1)–Ru(1)–O(2)	88.2(1)	O(1)–Ru(1)–O(3)	88.1(2)
O(2)–Ru(1)–O(3)	91.3(1)	O(1)–Ru(1)–N(1)	175.3(2)
O(2)–Ru(1)–N(1)	96.4(2)	O(3)–Ru(1)–N(1)	91.4(2)
O(1)–Ru(1)–N(2)	96.7(2)	O(2)–Ru(1)–N(2)	91.1(2)
O(3)–Ru(1)–N(2)	174.6(2)	N(1)–Ru(1)–N(2)	83.5(2)
O(1)–Ru(1)–N(3)	91.8(2)	O(2)–Ru(1)–N(3)	174.5(2)
O(3)–Ru(1)–N(3)	94.1(2)	N(1)–Ru(1)–N(3)	83.6(2)
N(2)–Ru(1)–N(3)	83.5(2)		
	Complex **4**		
Ru(1)–O(1)	1.913(1)	Ru(1)–N(1)	2.102(12)
Ru(1)–O(2)	2.039(8)	Ru(1)–N(2)	2.091(10)
Ru(1)–O(3)	2.051(9)	Ru(1)–N(3)	2.148(8)
O(1)–Ru(1)–O(2)	93.3(2)	O(2)–Ru(1)–N(2)	172.5(3)
O(1)–Ru(1)–O(3)	92.9(2)	O(3)–Ru(1)–N(2)	91.2(4)
O(2)–Ru(1)–O(3)	91.4(4)	N(1)–Ru(1)–N(2)	83.7(4)
O(1)–Ru(1)–N(1)	93.6(2)	O(1)–Ru(1)–N(3)	174.7(4)
O(2)–Ru(1)–N(1)	93.0(4)	O(2)–Ru(1)–N(3)	90.5(3)
O(3)–Ru(1)–N(1)	171.9(3)	O(3)–Ru(1)–N(3)	90.7(4)
O(1)–Ru(1)–N(2)	93.7(2)	N(1)–Ru(1)–N(3)	82.5(4)
Ru(1)–O(1)–Ru(1a)	180.0(1)	N(2)–Ru(1)–N(3)	82.4(4)

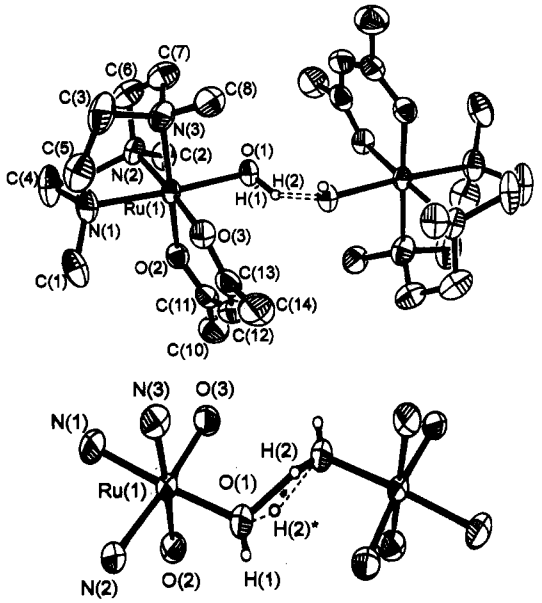

Figure 9. Structure of the dinuclear cation in crystals of **3** (top) and view of the first coordination sphere of the cation showing the $O_2H_3^-$ bridge with the disordered hydrogen atom H(2) (bottom). The asterisk denotes a crystallographic center of symmetry.

bond of the coordinated $H_3O_2^-$ bridge is significantly longer in **3** than the corresponding distance in **1** containing a terminal $H_3O_2^-$ ligand.

Crystals of **4** consist of the μ-oxo-bridged dinuclear cation $[\{LRu(acac)\}_2(\mu\text{-}O)]^{2+}$ and PF_6^- anions. The dication possesses crystallographically imposed C_i symmetry where the bridging oxygen O(1) lies on an inversion center. Consequentely, the Ru^{III}–O–Ru^{III} moiety is linear. The Ru–O_{oxo} bond distance of 1.913(1) Å is the longest observed to date for monooxo-bridged ruthenium(III) complexes (Table VII). The oxo bridge exerts a small but significant structural trans influence on the Ru–N bond in trans position with respect to the oxo group. Thus the difference $\Delta[(Ru\text{–}N_{trans})\text{–}(Ru\text{–}N_{cis})]$ is 0.05 Å.

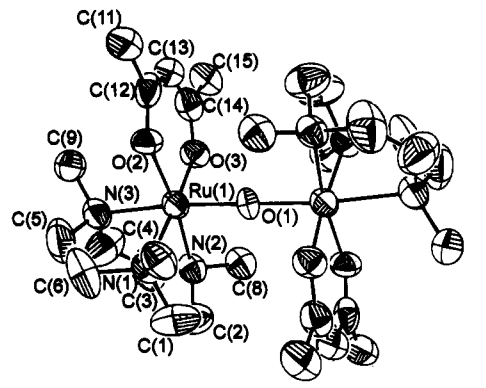

Figure 10. Structure of the dinuclear cation in crystals of **4**.

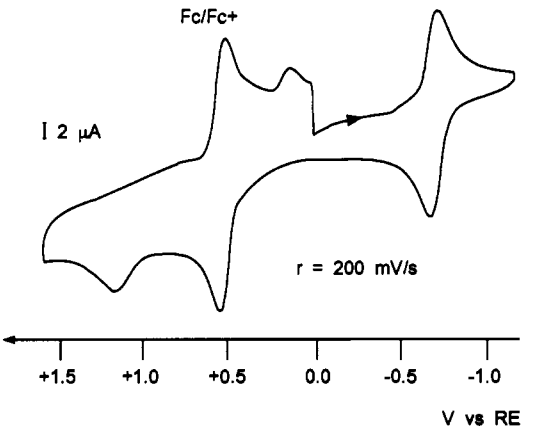

Figure 11. Cv of **1** in CH_3CN (0.10 M $[TBA]PF_6$) at a glassy-carbon working electrode with internal standard ferrocene (Fc). The reference electrode (RE) is Ag/AgCl (saturated LiCl in ethanol).

Electrochemistry. Figure 11 shows the cyclic voltammogram of $[LRu(acac)(H_3O_2)]PF_6$ (**1**) in acetonitrile containing 0.10 M $[TBA]PF_6$ supporting electrolyte at a glassy-carbon working electrode. A reversible one-electron wave at –0.85 V vs NHE ($E_{1/2}$) is observed which is assigned as the Ru^{III}/Ru^{II} couple (controlled-potential coulometry at –1.10 V vs Ag/AgCl, n = 1.04, ΔE_p = 52 mV, i_{pa}/i_{pc} = 1.02). During coulometry experiments a color change from orange to yellow is observed. The subsequent cv of such a reduced solution corresponds to the cv of a genuine sample of $[LRu^{II}(acac)(CH_3CN)]PF_6$,[31] which displays a reversible one-electron oxidation wave at +0.25 V vs NHE. Thus during the coulometry experiments substitution of the $H_3O_2^-$ ligand by acetonitrile occurs in the reduced form. In addition to the reversible Ru^{III}/Ru^{II} couple in the cv of **1** an irreversible one-electron oxidation peak at +1.05 V and an irreversible reduction peak at +0.02 V vs NHE is observed. Coulometry at +1.25 V vs NHE proved this oxidation to be a

(31) We have prepared diamagnetic yellow crystals of $[LRu^{II}(acac)(CH_3CN)]PF_6$ as follows: To a solution of **1** (0.05 g) in a water/acetonitrile mixture (1:1, 40 mL) was added $Na[BH_4]$ (0.20 g). The solution was heated reflux for 12 h under an argon-blanketing atmosphere. Addition of $NaPF_6$ initiated the precipitation of yellow $[LRu(acac)(CH_3CN)]PF_6$ in low yields (≈10%). Infrared (KBr disk), cm^{-1}: ν(C≡N) 2242. Anal. Calcd for $C_{16}H_{31}F_6N_4O_2PRu$: C, 34.5; H, 5.6; N, 10.1. Found: C, 34.2; H, 5.6; N, 9.9. Cyclic voltammogram (CH_3CN; 0.10 M $[TBA]PF_6$; glassy-carbon electrode): reversible one-electron wave at $E_{1/2}$ = +0.25 V vs NHE (ΔE_p = 60 mV; i_{pa}/i_{pc} = 0.98). 80 MHz ^1H NMR ($CDCl_3$; δ): 1.85 (s, 6H; C–CH_3), 2.35 (s, 3H; N–CH_3); 2.50 (s, 3H; $NCCH_3$); 2.82 (s, 6H; NCH_3), 2.88 (m, 12H, CH_2); 5.18 (s, 1H; CH).

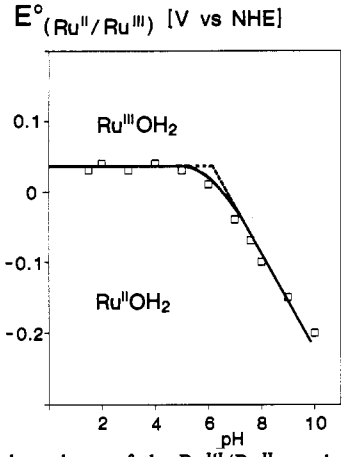

Figure 12. pH dependence of the Ru^{III}/Ru^{II} couple of **1** in aqueous buffer solutions at 20 °C.

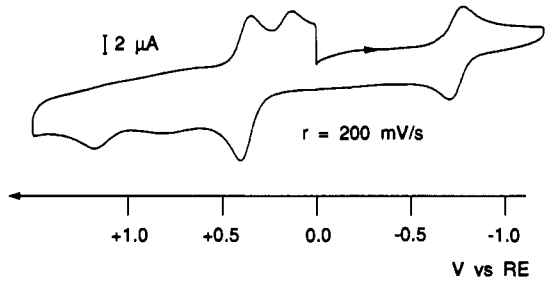

Figure 13. Cv of **3** in CH_3CN (0.10 M $[TBA]PF_6$; glassy-carbon electrode; Ag/AgCl reference electrode).

one-electron oxidation (n = 0.87). We tentatively assign this process to the formation of the oxoruthenium(IV) species $[LRu^{IV}(acac)(O)]^+$. Attempts to isolate this species from acetonitrile reaction mixtures of **1** with oxidants such as iodosobenzene, KIO_4, $Na[ClO_3]$, and $Na_2[S_2O_8]$ failed, although color changes were observed.

Figure 12 shows the pH dependence of the reversible Ru^{III}/Ru^{II} couple of **1** in aqueous buffer solutions at a glassy-carbon electrode. In the potential range +1.10 to −1.10 V vs NHE and a pH range 1–7 only the reversible one-electron wave is observed, at pH > 8 irreversible oxidation peaks are detected at ~0.65 V vs NHE. As the pH of the medium is raised, the formal redox potential shifts cathodically. The fact that the $E°$ for the Ru^{III}/Ru^{II} couple decreases by 60 mV per pH unit suggests that the Ru^{III}–O_2H_3 moiety is protonated by one proton yielding Ru^{II}–OH_2 upon reduction, eq 3. From the above electrochemistry a

$$[LRu^{III}(acac)(O_2H_3)]^+ + e^- + H^+ \rightleftharpoons [LRu^{II}(acac)(OH_2)]^+ + H_2O \quad (3)$$

pK_a value for the $[LRu^{III}(acac)(OH_2)]^{2+}$ species, eq 1, of 5.8 is calculated in excellent agreement with the spectrophotometrically determined value (Figure 1). Similar electrochemistry has been reported for *cis*- and *trans*-$[(terpy)(pic)Ru^{III}(H_2O)]^+$ [32] and $[(tmp)(bpy)Ru^{III}(H_2O)]^{2+}$,[33] where bpy = 2,2′-bipyridine, terpy = 2,2′:6′,2″-terpyridine, and tmp = tris(pyrazolyl)methane.

The cv of **3** (~10^{-3} M) in acetonitrile (0.10 M $[TBA]PF_6$) is displayed in Figure 13. It clearly shows that the dinuclear cation dissociates into an aquaruthenium(III) and a hydroxoruthenium(III) species since the former shows a reversible one-electron transfer wave at $E_{1/2}$ = +0.25 V vs NHE whereas the latter shows a similar reversible wave at $E_{1/2}$ = −0.86 V vs NHE and, in addition, an irreversible one-electron oxidation at +1.02 V and the corresponding reduction peaks at 0.01 V vs NHE which are assigned as above for the hydroxoruthenium(III) species (Scheme II).

Scheme II [a]

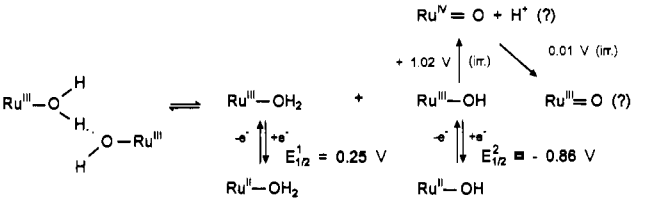

[a] Potentials are referenced vs NHE.

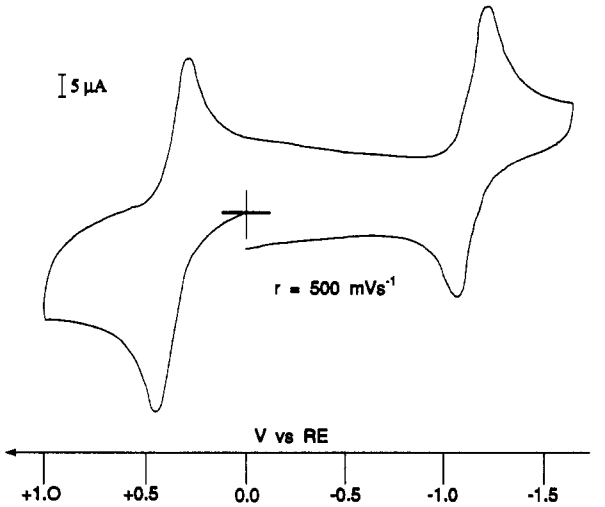

Figure 14. Cv of **4** in CH_3CN (0.10 M $[TBA]PF_6$; glassy-carbon electrode; Ag/AgCl reference electrode).

The cv of **4** in acetonitrile (0.10 M $[TBA]PF_6$) displays two reversible one-electron transfer waves at $E_{1/2}$ values of +0.25 and −1.23 V vs NHE (Figure 14) in the potential range +1.7 to −1.7 V vs NHE. These are assigned to the couples $Ru^{IV}Ru^{III}/Ru^{III}_2$ and $Ru^{III}_2/Ru^{III}Ru^{II}$, respectively.

Discussion

The present series of mono- and dinuclear complexes containing the five-coordinate LRu(acac) fragment allows a detailed comparison of structural and electronic properties as the nature of the sixth ligand is varied from terminal aqua or hydroxo to briding ($H_3O_2^-$) or oxo ligands.

Complex **1** is of interest because it represents one of the few structurally characterized octahedral hydroxoruthenium complexes. *trans*-$Na_2[Ru(NO_2)_4(NO)(OH)]\cdot 2H_2O$[34] and *trans*-$[RuL'(OH)(NO)](ClO_4)$[35] (L′ = 1,5,9,13-tetramethyl-1,5,9,15-tetraazacyclohexadecane) have short $Ru–O_{hydroxo}$ bond lengths of 1.962(2) and 1.909(2) Å, respectively, as compared to Ru–OH_2 bonds. The hydroxo groups are not hydrogen bonded to water molecules. It is a well-known spectroscopic problem concerning the position of the hydroxo group in the spectrochemical series. This is due to the fact that M–OH moieties rarely exist as such in polar solvents and almost certainly not in water. In the case of **1** the $H_3O_2^-$ ligand is present in both the solid state and probably in aqueous solution.

Complex **3** contains the more common bridging $H_3O_2^-$ moiety[36] although it is clearly not of the symmetrical type, where the proton of the O–H···O group is equidistant to both oxygen atoms. Since the cation in **3** possesses crystallographic site symmetry C_i, it is not possible to establish whether this asymmetry leads to two different Ru^{III}–O distances or whether a dynamic process (proton

(32) Llobet, A.; Doppelt, P.; Meyer, T. J. *Inorg. Chem.* **1988**, *27*, 514.
(33) Llobet, A.; Hodgson, D. J.; Meyer, T. J. *Inorg. Chem.* **1990**, *29*, 3760.
(34) Blake, A. J.; Goud, R. O.; Johnson, B. F. G.; Parisini, E. *Acta Crystallogr., Sect. C* **1992**, *C48*, 982.
(35) Wong, K.-Y.; Che, C.-M.; Yip, W.-H.; Wang, R.-J.; Mak, T. C. W. *J. Chem. Soc., Dalton Trans.* **1992**, 1417.
(36) An excellent review on the bridging $H_3O_2^-$ ligand has appeared: Ardon, M.; Bino, A. *Structure and Bonding*; Springer-Verlag: Berlin, Heidelberg, 1987; Vol. 65.

Table VII. Structural Data for $M(\mu\text{-}O_2H_3)M$ Complexes

complex	O···O, Å	M–O, Å	M···M, Å	∠M–O–H, deg	∠O–H···O, deg	∠H–O–H, deg	ref
$[\{LRu^{III}(acac)\}_2(\mu\text{-}O_2H_3)]^{3+}$	2.494(7)	2.043	5.70	115	117	93	this work
$[\{LCr^{III}(acac)\}_2(\mu\text{-}O_2H_3)]^{3+}$	2.496(6)	1.969	5.58	107 119	180	115	19b
trans-$[Ru^{III}(bpy)_2(OH_2)(OH)]^{2+}$	2.538(7)	2.007	5.79	110 125	169	113	37a
trans-$[(Co^{III}(en)_2)(O_2H_3)]_n^{2n+}$	2.441	1.916	5.72	111 130	180	106	37b

Table VIII. Comparison of Electronic, Magnetic, and Structural Properties of μ-Oxo-Bridged Complexes[a]

complex	$Ru\text{–}O_{oxo}$, Å	Ru–O–Ru, deg	λ_{max}, nm (ϵ, L·mol^{-1} cm^{-1})	magnetism[b]	ref
$[\{(NH_3)_5Ru^{III}\}_2O]^{4+}$			503 (1.6×10^4)[c]	2.1 μ_B (293 K), 0.5 μ_B (18 K)	4
$[\{(NH_3)_5Ru^{3.5}\}_2O]^{5+}$			342 (2.5×10^4)		4
$[\{LRu^{III}(acac)\}_2O]^{2+}$	1.913(1)	180	596 (1.24×10^4)	a.f. $J = -53$ cm^{-1}	this work
$[\{LRu^{3.5}(acac)\}_2O]^{3+}$			537 (5.7×10^3)	1.6 μ_B (295 K)	this work
$[\{(bpy)_2(H_2O)Ru^{III}\}_2O]^{4+}$	1.869(1)	165.4(3)	660 (2.5×10^4)		7
$[\{(bpy)_2(NO_2)Ru^{III}\}_2O]^{2+}$	1.890(7) 1.876(6)	157.2(3)	632 (2.57×10^4)	a.f. $J = -86.5$ cm^{-1}	5, 8
$[\{(phen)_2(NO_2)Ru^{III}\}_2O]^{2+}$			640 (2.53×10^4)	a.f. $J = -60$ cm^{-1}	5, 8
$[\{(edta)Ru^{3.5}\}_2O]^{3-}$		~165 (est.)	392 (1.79×10^4)	2.10 μ_B (296 K)	9, 11
$[L_2Ru^{III}_2(O)(\mu\text{-}CH_3CO_2)_2]^{2+}$	1.884(2)	119.7(2)	542 (6.1×10^3)	diamagnetic	28
$[L_2Ru^{3.5}_2(O)(\mu\text{-}CH_3CO_2)_2]^{3+}$	1.837(5) 1.849(5)	130.1(3)	478 (5.7×10^3)	2.0 μ_B (298 K)	28
$[\{(OEP)ClRu^{IV}\}_2O]$	1.793(2)	180	690 (1.0×10^4)[d]	diamagnetic	12a
$[\{(OEP)(OH)Ru^{IV}\}_2O]$	1.847(13)	180	580 (2.09×10^4)[d]	diamagnetic	12b
$[\{Cl_5Ru^{IV}\}_2O]^{4-}$	1.80	180		diamagnetic	13

[a] Abbreviations: acac = pentane-2,4-dionate; L = 1,4,7-trimethyl-1,4,7-triazacyclononane; bpy = 2,2′-bipyridine; phen = 2,2′-phenanthroline; edta = ethylenediaminetetraacetate; OEP = octaethylporphinate; a.f. = antiferromagnetic. [b] Magnetic moments are per dinuclear unit. J convention: $H = -2JS_1S_2$. [c] Solvent: acetonitrile unless indicated otherwise. [d] Solvent: CH_2Cl_2.

hopping) prevails in the solid state.

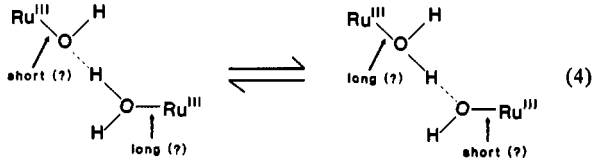

(4)

Symmetrical bridging $H_3O_2^-$ units between ruthenium(III) ions have been characterized by X-ray crystallography previously for *trans*-$[Ru^{III}(bpy)_2(OH)(OH_2)](ClO_4)_2$,[37] which is a linear $O_2H_3^-$-bridged polymer. Table VII summarizes some structural data of $O_2H_3^-$-bridged complexes. The O–H···O bonds in **1** and **3** are borderline between strong and very strong according to Ardon and Bino's classification[36] and the corresponding H-bond energy is between 100 and 50 kJ/mol. Complex **1** represents the first example of a coordinated terminal $O_2H_3^-$ ligand.

It is quite remarkable that solid **1** reacts *in vacuo* at elevated temperature with elemination of water by generating the (μ-oxo)diruthenium(III) complex **4** (eq 5). Part of the driving force

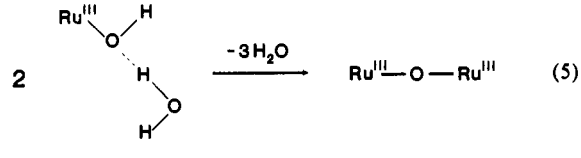

(5)

for reaction 5 stems from the formation of a thermodynamically very stable Ru^{III}–O–Ru^{III} moiety. Stoichiometry considerations would imply the formation of a Ru–OH–Ru unit from water elimination from **3**. This unit is thermodynamically less stable and has in fact not been observed in ruthenium(III) chemistry. Thus reaction 6 has not been observed to date.

Table VIII gives structural, electronic spectral, and magnetic properties for dinuclear complexes of ruthenium(III) and -(IV) for comparison. Two types of complexes will be considered here:

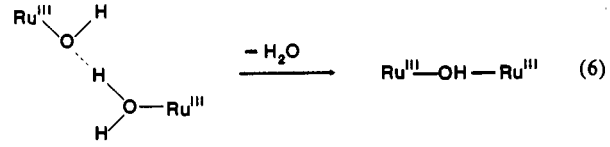

(6)

the singly and triply bridged species A and B, the latter of which has only recently begun to appear in the literature.[28,38-42]

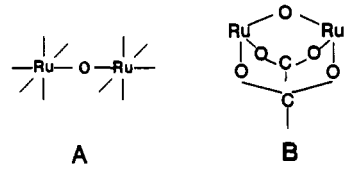

For the singly bridged (μ-oxo)diruthenium(III) complexes the following structural features appear to be general. The Ru–O–Ru angle spans a range from 157.2 to 180°. Thus bent and a linear species have now been characterized. We propose that this is a consequence of the steric congestion introduced by the coordinated acac ligand at one Ru atom and a methyl group of the cyclic triamine at the other Ru ion. It is interesting in this respect that the analogous diiron(III) complex $[L''_2Fe^{III}_2(acac)_2(\mu\text{-}O)](ClO_4)_2$, where L″ represents the unmethylated derivative of L, namely 1,4,7-triazacyclononane, is bent (Fe–O–Fe = 158.6°). This is in contrast to (μ-oxo)diruthenium(IV) species all of which appear to contain a strictly linear Ru^{IV}–O–Ru^{IV} unit. The steric requirements of the ligands in **4** enforce not only a linear Ru–O–Ru unit but also somewhat elongated $Ru\text{–}O_{oxo}$ bond lengths, which is 1.88 Å in all complexes without steric interactions between ligands but 1.913(1) Å in **4**.

(37) (a) Durham, B.; Wilson, S. R.; Hodgson, D. J.; Meyer, T. J. *J. Am. Chem. Soc.* **1980**, *102*, 600. (b) Ardon, M.; Bino, A. *Inorg. Chem.* **1985**, *24*, 1343.

(38) Neubold, P.; Wieghardt, K.; Nuber, B.; Weiss, J. *Angew. Chem., Int. Ed. Engl.* **1988**, *27*, 933.

(39) Sasaki, Y.; Suzuki, M.; Tokiwa, A.; Ebikara, M.; Yamaguchi, T.; Kabuto, C.; Ito, T. *J. Am. Chem. Soc.* **1988**, *110*, 6251.

(40) Llobet, A.; Curry, M. E.; Evans, H. T.; Meyer, T. J. *Inorg. Chem.* **1989**, *28*, 3131.

(41) Das, B. K.; Chakravarty, A. R. *Inorg. Chem.* **1990**, *29*, 2078.

(42) Das, B. K.; Chakravarty, A. R. *Inorg. Chem.* **1991**, *30*, 4978.

This effect is real as is seen by the reduced exchange coupling in **4** as compared to $[\{(bpy)_2(NO_2)Ru^{III}\}_2(\mu\text{-}O)]^{2+}$,[5,8] for which J values of -53 and -86.5 cm^{-1} have been observed, respectively. Magnetic exchange coupling via a superexchange pathway in M–O–M complexes is predominantly governed by the M–O_{oxo} bond distance. Gorun and Lippard[43] have recently reported a correlation between the distance and the magnitude of J for some dinuclear complexes containing a (μ-oxo)diiron(III) core, eq 7,

$$-J = A \exp(BP) \qquad (7)$$

where $A = 8.763$ and $B = -12.663$ and P is the average shortest distance between the metals and the oxo ligand. Thus, an exponential decrease of the antiferromagnetic coupling with increasing M–O_{oxo} bond distance is observed. In a very crude model we assume this correlation to hold also for the two other singly bridged ruthenium(III) complexes[5,8] and **4**. Taking into account the difference of the ionic radii of six-coordinate low-spin ruthenium(III) (0.82 Å) and high-spin iron(III) (0.785 Å),[44] we convert the observed Ru–O_{oxo} distances into analogous "Fe–O_{oxo}" distances by subtracting 0.035 Å and using these corrected values to calculate J-values by using eq 7. We arrive at -41 cm^{-1} for **4** and -60 cm^{-1} for $[\{(bpy)_2(NO_2)Ru^{III}\}_2(\mu\text{-}O)]^{2+}$. Although the numerical agreement with observed data is poor, it is interesting that the calculated energy difference of 19 cm^{-1} reproduces qualitatively the observed of 33 cm^{-1}. This may imply that a similar correlation between Ru–O_{oxo} bond distances and J-values holds as for the diiron(III) complexes and, if this is true, that the same π-superexchange pathway prevails in both series of compounds.

It is quite revealing that the exchange coupling in the triply bridged diruthenium(III) complexes is considerably *stronger* than in the singly bridged species despite the fact that the Ru–O_{oxo} bonds are also 1.88 Å. For the analogous diiron(III) complexes this has not been observed.[45] We take this as an indication that in the triply bridged diruthenium(III) complexes the mechanism of exchange coupling has changed. We have previously proposed that a direct metal–metal interaction may account for the observed diamagnetism of these complexes.[28,38]

Since Meyer et al's[5] original proposal following Dunitz and Orgel,[46] it has become customary to describe the bonding of Ru–O–Ru units by using a delocalized MO scheme shown in Figure 15. Due to bending of the Ru–O–Ru unit or low symmetry of the corner-sharing octahedra, the degeneracy of the $\pi_1^*\pi_2^*$ and

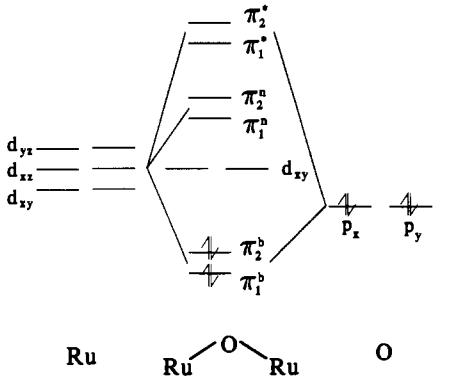

Figure 15. Qualitative molecular orbital scheme for a bent Ru–O–Ru system (adapted from refs 2a and 5).

$\pi_1^n\pi_2^n$ orbitals is assumed to be lifted. In Ru^{III}–O–Ru^{III} species the π_1^* orbital is then the HOMO. Removal of one electron from the π_1^* orbital generates a delocalized $Ru^{3.5}$–O–$Ru^{3.5}$ unit with one delocalized unpaired electron ($S = {}^1/_2$) whereas oxidation to Ru^{IV}–O–Ru^{IV} unit renders the π^* antibonding orbitals empty. This picture correctly accounts for the shortening of Ru–O_{oxo} bond distances on going from $Ru^{III}_2(\mu\text{-}O)$ to $Ru^{3.5}_2(\mu\text{-}O)$ to $Ru^{IV}_2(\mu\text{-}O)$ complexes and for the observed electronic ground states of $S = 0$, $S = {}^1/_2$, and $S = 0$, respectively. On the other hand, it should be kept in mind that a description using localized metal orbitals with only a small perturbation by the filled orbitals of the O^{2-}-bridge also accounts correctly for all these properties. A superexchange mechanism mediated by an oxo bridge between low-spin ruthenium(III) ions ($S = {}^1/_2$) and/or ruthenium(IV) ($S = 1$) is a valid picture to describe the magnetic and electronic properties of complexes **4** and **5**. For a more detailed discussion of this point, see ref 47.

Acknowledgment. We thank the Fonds der Chemischen Industrie for financial support. We are grateful to Degussa, Hanau, Germany, for a generous loan of $RuCl_3 \cdot nH_2O$. We thank Professor A. X. Trautwein, Dr. E. Bill, and Dipl.-Phys. C. Butzlaff (Medizinische Universität Lübeck) for measuring the ESR spectra and temperature-dependent magnetic susceptibility data.

Supplementary Material Available: Tables listing additional details of the structure determinations, anisotropic thermal parameters, hydrogen atom coordinates, and bond angles and distances for complexes **1**, **3**, and **4** (20 pages). Ordering information is given on any current masthead page.

(43) Gorun, S. M.; Lippard, S. J. *Inorg. Chem.* **1991**, *30*, 1625.
(44) Shannon, R. D. *Acta Crystallogr., Sect. A* **1976**, *A32*, 751.
(45) Kurtz, D. M., Jr. *Chem. Rev.* **1990**, *90*, 585.
(46) Dunitz, J. D.; Orgel, L. E. *J. Chem. Soc.* **1953**, 2594.
(47) Hotzelmann, R.; Wieghardt, K.; Flörke, U.; Haupt, H.-J.; Weatherburn, D. C.; Bonvoisin, J.; Blondin, G.; Girerd, J.-J. *J. Am. Chem. Soc.* **1992**, *114*, 1681.